Biochemical Journal (2020) **477** 275–284
https://doi.org/10.1042/BCJ20190196

PORTLAND PRESS

Research Article

The structure of human GCN2 reveals a parallel, back-to-back kinase dimer with a plastic DFG activation loop motif

Taiana Maia de Oliveira[1], Victoria Korboukh[2], Sarah Caswell[3], Jon J. Winter Holt[4], Michelle Lamb[5], Alexander W. Hird[5] and Ross Overman[3]

[1]Structure, Biophysics and FBLG, Discovery Sciences, R&D, AstraZeneca, Cambridge, UK; [2]Mechanistic Biology and Profiling, Discovery Sciences, R&D, AstraZeneca, Boston, US; [3]Discovery Biology, Discovery Sciences, R&D, AstraZeneca, Cambridge, UK; [4]Medicinal Chemistry, Oncology R&D, AstraZeneca, Cambridge, UK; [5]Medicinal Chemistry, Oncology R&D, AstraZeneca, Waltham, MA, USA

Correspondence: Taiana Maia de Oliveira (taiana.maiadeoliveira@astrazeneca.com)

When activated by amino acid starvation, the stress sensing protein kinase GCN2 phosphorylates the eukaryotic initiation factor 2 alpha, inhibiting translation to conserve energy and facilitate cell survival. Amino acid starvation, particularly of tryptophan and arginine, affects immune tolerance by suppressing differentiation and proliferation of T-cells via activation of GCN2 kinase. In addition, the GCN2 pathway mediates cancer survival directly within the context of metabolic stress. Here, we report the first crystal structures of the human GCN2 kinase domain (KD) in complex with two inhibitors of different size, shape, and chemical scaffold. Three novel activation loop conformations representative of different activation states of the kinase are described. In addition, a novel dimerization organization for GCN2 is observed. This arrangement is consistent with the hypothesis that the GCN2 KD forms an antiparallel inactive dimer until uncharged tRNA binds to it and triggers conformational changes that shift the equilibrium to the active parallel dimer.

Introduction

GCN2, general control nonderepressible 2 kinase, is one of four known vertebrate kinases — GCN2, PERK, PKR, and HRI — that respond to cellular stress by deactivating the eukaryotic initiation factor 2 alpha (eIF2α). More specifically, GCN2 acts as a metabolic sensor by binding to uncharged tRNA, whose levels are enhanced by nutrient starvation, and eliciting amino acid deficiency stress response via phosphorylation of Serine 51 of eIFα2, which culminates in a reduction in overall translation. This adaptive response saves energy and regulates signaling pathways to facilitate survival [1].

Numerous studies implicate GCN2 as instrumental to medically relevant events as diverse as cancer immune evasion and long-term memory formation. In fact, GCN2 has a dual pertinence in cancer biology: in addition to the suppressing of T cell differentiation that supports immune tolerance within the tumor microenvironment; as a stress response kinase, it promotes tumor survival and aggressiveness by maintaining tumor metabolic homeostasis [2].

The molecular mechanism of GCN2 activation is elusive and intricate as it results from the interplay of five defined domains of the protein: a RWD region that acts as a regulatory site, a PKD (pseudokinase domain), a KD (kinase domain), a HisRS (histidyl-tRNA synthetase) related domain that binds uncharged tRNA and a CTD (C-terminal dimerization domain) that in addition contributes to tRNA binding [3]. Moreover, ribosome binding has also been implicated in the activation of GCN2 [4]. To date, structural information on GCN2 has been limited to the yeast and murine CTD [5], the yeast KD [6], and the murine RWD [7]. The crystal structure of the CTD shows an interdigitated intimately connected dimer in which its core beta sheet is formed through interactions of strands

Received: 11 March 2019
Revised: 10 December 2019
Accepted: 23 December 2019

Accepted Manuscript online: 23 December 2019
Version of Record published: 17 January 2020

Biochemical Journal (2020) 477 275–284
https://doi.org/10.1042/BCJ20190196

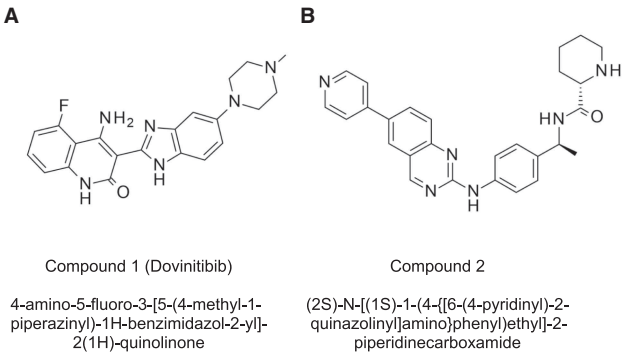

Figure 1. Chemical structures of GCN2 binding compounds co-crystallized with human GCN2.
(**A**) Compound 1 or dovitinib and (**B**) Compound 2 or (2S)-N-[(1S)-1-(4-{[6-(4-pyridinyl)-2-quinazolinyl]amino}phenyl)ethyl]-2-piperidinecarboxamide.

from both polypeptide chains [5]. This supports the hypothesis that GCN2 is a constitutive dimer and activation upon tRNA binding would require a conformational change from the auto-inhibited state into the active one. Previous reports also implicate the KD and HisRS domain in the mediation of dimerization [8,6]. In addition, the PKD of interacts with the catalytic KD domain and inhibits its catalytic activity under non-starvation conditions [9].

Currently, the structural notions surrounding the mechanisms of eIF2α kinases derive mainly from the crystal structures of the human PKR KD in complex with eIF2α [10], yeast GCN2 KD in the hyperactive and native form [6], and human PERK KD [11]. Recognition of eIF2α by these proteins seems to be achieved by a noncanonical orientation of the helix αG that accommodates eIF2α by an induced fit mechanism that exposes its previously buried Ser51, allowing it to be phosphorylated [12]. Curiously, in these structures PKR organizes itself in a parallel dimer while, the yeast GCN2 is markedly different, being organized as an antiparallel dimer through N-lobe interactions [13].

Here, we report the first crystal structures of the human GCN2 KD in complex with two inhibitors of different size, shape, and chemical scaffold (Figure 1). In addition, three activation loop conformations representative of different activation states of the kinase are described. We show a range of conformational states can be stabilized by different ligands bound to the ATP binding pocket. This diversity can be potentially exploited for the development of conformation selective inhibitors for the treatment of cancer. Finally, these structures reveal a novel dimerization organization for GCN2 consistent with the hypothesis that the GCN2 KD would exist as an antiparallel inactive dimer until uncharged tRNA binds to it and triggers conformational changes that shift the equilibrium to the active parallel dimer.

Materials and methods

Molecular biology

For crystallographic studies, the constructs for the human eIF2α kinase GCN2 (UniProtKB — Q9P2K8, E2AK4_HUMAN) were synthesized by GeneArt (Thermo Fisher Scientific) and cloned into a modified version of the pET28b vector. All constructs contained an N-terminal His6 tag followed by a TEV protease cleavage site upstream of the KD sequence (S577-T1020), together with an internal deletion to remove A663-P788 of the N-terminal lobe insertion region. In addition, one construct contained a D848N mutation to catalytically inactivate the kinase, and a second contained both T899A and T904A mutations to remove putative autocatalytic sites [14]. Protein sequences used for both constructs in this study are shown below.

6His-TEV-GCN2(S577-T1020,ΔA663-P788)

MHHHHHHGGGENLYFQGSSETQRQFSRYFIEFEELQLLGKGAFGAVIKVQNKLDGCCYAVKRIPINPASRQ-FRRIKGEVTLLSRLHHENIVRYYNAWIERHERPSVTTEAVHYLYIQMEYCEKSTLRDTIDQGLYRDTVRLWR-LFREILDGLAYIHEKGMIHRDLKPVNIFLDSDDHVKIGDFGLATDHLAFSADSKQDDQTGDLIKSDPSGHLT-GMVGTALYVSPEVQGSTKSAYNQKVDLFSLGIIFFEMSYHPMVTASERIFVLNQLRDPTSPKFPEDFDDGEH-AKQKSVISWLLNHDPAKRPTATELLKSELLPPPQMEESELHEVLHHTLT

Biochemical Journal (2020) 477 275–284
https://doi.org/10.1042/BCJ20190196

PORTLAND PRESS

6His-TEV-GCN2(S577-T1020,ΔA663-P788,D848N)

MHHHHHHGGGENLYFQGSSETQRQFSRYFIEFEELQLLGKGAFGAVIKVQNKLDGCCYAVKRIPINPASRQ-
FRRIKGEVTLLSRLHHENIVRYYNAWIERHERPSVTTEAVHYLYIQMEYCEKSTLRDTIDQGLYRDTVRLWR-
LFREILDGLAYIHEKGMIHRNLKPVNIFLDSDDHVKIGDFGLATDHLAFSADSKQDDQTGDLIKSDPSGHLT-
GMVGTALYVSPEVQGSTKSAYNQKVDLFSLGIIFFEMSYHPMVTASERIFVLNQLRDPTSPKFPEDFDDGEH-
AKQKSVISWLLNHDPAKRPTATELLKSELLPPPQMEESELHEVLHHTLT

6His-TEV-GCN2(S577-T1020,ΔA663-P788, T899a,T904A)

MHHHHHHGGGENLYFQGSSETQRQFSRYFIEFEELQLLGKGAFGAVIKVQNKLDGCCYAVKRIPINPASRQ-
FRRIKGEVTLLSRLHHENIVRYYNAWIERHERPSVTTEAVHYLYIQMEYCEKSTLRDTIDQGLYRDTVRLWR-
LFREILDGLAYIHEKGMIHRDLKPVNIFLDSDDHVKIGDFGLATDHLAFSADSKQDDQTGDLIKSDPSGHLA-
GMVGAALYVSPEVQGSTKSAYNQKVDLFSLGIIFFEMSYHPMVTASERIFVLNQLRDPTSPKFPEDFDDGEH-
AKQKSVISWLLNHDPAKRPTATELLKSELLPPPQMEESELHEVLHHTLT

Mass spectrometry analysis for phosphorylation state

To obtain quantifiable phosphorylation data, kinase samples at 1 mg/ml in final buffer were loaded onto a Micromass LCT ES-TOF (liquid chromatography electrospray ionization time-of-flight) mass spectrometer, using a Waters 2790 HPLC as the inlet. Fifteen micrograms of protein was injected for each measurement onto a Phenomenex Jupiter 5 m C5 300A column, 150 × 2.0 mm. Protein was eluted using a fast gradient (0–90% B over 45 min at 120 ml/min; eluent A was aqueous 0.1% TFA, eluent B was 90% acetonitrile 0.1% TFA). Electrospray mass spectrometer data were collected between 12 and 25 min post injection, and deconvoluted using MaxEnt1 software (Waters). Theoretical protein masses were calculated using the MassLynx™ software (Waters).

Biochemical activity assay

Reagents

GFP-eIF2S1 and Tb-anti-peIF2alpha [pSer52] antibody were from ThermoFisher (PV4809 & PV4815, respectively), *Escherichia coli* tRNA was from Roche, sold by Sigma (10109541001).

Protein constructs used

G-GCN2-(S577-T1020, dA663-P788), ∼7 phosphorylation sites.
GSGGG-6His-GCN2 (S572-G1024)-Avi, phosphorylated (10–15 sites)
6His-GCN2 (S572-G1024)-Avi, has ∼5 phosphorylation sites.
GSGGG-6His-GCN2 (S572-G1024)-Avi, dephosphorylated.
Full-length GCN2 (lack of threonine 899 phosphorylation confirmed by Western Blot.

Experimental part

In brief, 1 μl of 2× GCN2 solution in 1× reaction buffer (20 mM Tris pH 7.5, 5 mM $MgCl_2$, 1 mM DTT, 0.005% Brij-35, and 0.5 mM EGTA) was added to a 1536-well plate (20 and 5 nM final concentration in 2 μl reaction for KD and FL construct, respectively). Reactions were initiated by adding 1 μl of 2× ATP/GFP-eIF2S1 (100 μM/25 nM final concentration) and ATP/tRNA/GFP-eIF2S1 (100 μM/0.2 mg/ml/25 nM final concentration) for one of the FL reactions. Plates were gently tapped to assure proper mixing of reagents. Reactions were then incubated for indicated time periods and quenched by the addition of 0.5 μl EDTA solution to final concentration of 20 mM (in 1× reaction buffer + 0.15% BSA). After the last time point, 0.5 μl of antibody solution (in 1× reaction buffer + 0.15% BSA) was added to all wells to 2 nM final concentration. To ensure proper mixing of reagents plate was first gently tapped and then spun for 1 min at 1000 rpm at RT. Plate was then sealed and incubated for 90 min at RT in the dark. Plates were then read on a BMG PHERAstar FSX (Ex.340, Em. 490/520, fly mode).

IC50 determination

Twenty nanoliters of compounds covering concentration range from 30 μM to 1 nL were added to 1536 well plates (Greiner 782075). One microliter of 2× GCN2 solution in 1× reaction buffer (20 mM Tris pH 7.5, 5 mM $MgCl_2$, 1 mM DTT, 0.005% Brij-35, and 0.5 mM EGTA) was added to each well of a 1536-well plate (1 nM

Biochemical Journal (2020) 477 275–284
https://doi.org/10.1042/BCJ20190196

final concentration in 2 μl final volume). Reactions were initiated by adding 1 μl of 2× ATP/tRNA/GFP-eIF2α (100 μM/0.2 mg/ml/25 nM final concentration). Plates were gently tapped to ensure proper mixing of reagents. Reactions were then incubated for 70 min at RT and quenched by addition of 1 μl 3× quench solution (3 μM of potent GCN2 inhibitor 4-(5-((1-(tetrahydro-2H-pyran-4-yl)-1H-pyrazol-4-yl)amino)-3H-[1,2,3]triazolo [4,5d]pyrimidin-3-yl) benzamide, 6 nM p-GFP-EIF2α (phospho S52) Tb-Antibody 0.15% BSA in reaction buffer). To ensure proper mixing of reagents plates were gently tapped and then sealed and incubated for 90 min at RT in the dark. Plates were then read on a BMG PHERAstar FSX (Ex.340, Em. 490/520, fly mode). For artifact plates 2 μl of fully phosphorylated GFP-eIF2α solution (1.5 nM) were added to compound wells, followed by 1 μl of 3× quench solution. Data were analyzed using Genedata Screener, for artifact plates to correct for compound fluorescence correction, a two-point normalization based on central (Neutral) and scale reference (stimulator/inhibitor control) well types correction was performed [15] In brief, it attempts to correct for the interference caused by compounds by either subtracting excess signal or by multiplying to add back reduced signal measured in separate compound-only plate (artifact plate). Correction of the assay plates by the artifact plates is limited to a two-fold correction (increase or decrease in signal). If the compound interference exceeds this limit, the well in question is masked for the purposes of fitting.

Protein expression and purification

The 6His-TEV-GCN2(S577-T1020, ΔA663-P788,D848N) construct was transformed into BL21 GOLD (DE3) cells (Agilent Technologies) and expressed overnight at 18°C, using 0.1 mM IPTG. Cell pellets were resuspended in a lysis buffer consisting of 40 mM HEPES pH 8.0, 500 mM NaCl, 1 mM TCEP, 20 mM imidazole, Benzonase® Nuclease (Merck KGaA) and cOmplete EDTA-free protease inhibitors (Roche) and lysed by a single pass through a cell disruptor (Constant Systems Ltd) at 25 kpsi. The cell lysate was clarified by centrifugation at 70 000×***g*** and proteins purified from the supernatant by batch-binding using Ni-NTA Superflow (QIAGEN). Following elution in 40 mM HEPES pH8.0, 300 mM NaCl, 1 mM TCEP, 500 mM imidazole, the N-terminal His6 tag was removed by overnight dialysis (40 mM HEPES pH8.0, 300 mM NaCl, 0.5 mM TCEP) in the presence of TEV protease (3 mg TEV/100 mg target protein). Samples were further purified by reverse IMAC followed by size exclusion chromatography using a Superdex 75 column (GE Healthcare) into a final buffer composed of 40 mM HEPES pH 7.9, 200 mM NaCl, 1 mM TCEP. An identical purification method was followed for 6His-TEV-GCN2(S577-T1020,ΔA663-P788) and 6His-TEV-GCN2(S577-T1020,ΔA663-P788, T899A,T904A), however, the latter construct was co-expressed with full length, untagged Lambda Protein Phosphatase (UniProtKB — P03772) on a pCDF-1b plasmid (Novagen), using *E. coli* BL21 Star™ (DE3) cells (Thermofisher).

Crystallization of human GCN2 KD

The protein samples used for crystallization were concentrated to 9 mg/ml in the purification buffer 40 mM HEPES pH 7.9, 200 mM NaCl, 1 mM TCEP. The compounds were added to final concentration of 50 μM (5% DMSO-Protein-Buffer) incubated for 30 min and centrifuged for 10 min at 9000***g*** before plates were setup. Crystals were obtained by the hanging-drop vapor-diffusion method under conditions consisting of 0.1 M MES pH 6, 20% PEG 8000 with 0.2 M calcium acetate (GCN2 + dovitinib) and 0.1 M BIS-TRIS pH 5.5–6.5, 20–25% PEG335 with 0.2 M ammonium sulfate (GCN2+(2S)-N-[(1S)-1-(4-{[6-(4-pyridinyl)-2-quinazolinyl]amino} phenyl)ethyl]-2 piperidinecarboxamide at room temperature. The drops were composed of 2 μl of the protein-compound mixture and 2 μl of the well solution. Finally, the crystals were soaked in cryoprotectant consisting of 25% ethylene glycol and immediately frozen in liquid nitrogen.

Data collection and structure determination

Diffraction data from the GCN2 crystals were collected remotely at the Diamond Beamline I04. Data were integrated with XDS, scaled with AIMLESS and the structures were determined by the molecular-replacement method using the program MolRep. The models of GCN2 KD were manually built using COOT [16] and further refined using BUSTER [17]. X-ray data collection and refinement statistics are presented in Table 1. The structure of GCN2:aminoquinazoline at 2.3 Å resolution displays R_{factor} and R_{free} of 0.21 and 0.24 while the structure of GCN2:dovinitib at 2.8 Å resolution displays R_{factor} and R_{free} of 0.21 and 0.26. The relatively large difference between *R* factor and *R* free of the latter is probably a consequence of the resolution. No residues are in the disallowed region.

Table 1 X-ray data collection and refinement statistics

	GCN2:dovinitib	GCN2:aminoquinazoline
Space group	$C222_1$	P1
Cell dimensions		
a, *b*, *c* (Å)	*a* = 155, *b* = 162, *c* = 123	*a* = 73.8, *b* = 77.79, *c* = 101.69
α, β, γ (°)	90, 90, 90	89.86, 90.05, 68.58
Resolution (Å)	49.36–2.8	2.3
R_{merge}	0.11	0.07 (0.67)
$I/\sigma I$	10.7 (0.9)	3.6 (0.9)
Completeness (%)	99.5 (94.1)	96.3 (85)
Number of reflections	38 997	90 485
R_{factor}/R_{free}	0.21/0.24	0.21/0.24

Results and discussion

Crystallization of human GCN2

As seen in other eIF2α kinases, GCN2 features a unique loop inserted within the N-lobe of the KD. However, in GCN2, the loop is over 100 amino acids long and was thus engineered out of the crystallizable constructs (Δ663–788). Optimization of domain boundaries was based on sequence alignments, secondary structure prediction, and analysis of the yeast GCN2 and human PERK structures. Construct 6His-TEV-GCN2(S577-T1020, ΔA663-P788) was expressed in *E. coli* but MS analysis revealed the protein to be highly autophosphorylated (Supplementary Figure S1). We opted then to introduce inactivating mutations at the catalytic loop and at the activation loop and expressed the following (respectively): GCN2 S577-T1020, ΔA663-P788, D848N and GCN2 S577-T1020, ΔA663-P788, T899A, T904A. Sample homogeneity was accessed by SEC-MALS (Supplementary Figure S2) and activity was probed by a biochemical assay (Supplementary Figure S3) as described in the Supplementary Methods

This allowed us to obtain stable protein, which was, however, still refractory to crystallization in the absence of ligands. Pre-incubation of GCN2 S577-T1020, ΔA663-P788, D848N and S577-T1020 construct with Dovitinib (Compound 1; IC_{50} 0.9 μM) and GCN2 S577-T1020, ΔA663-P788,T899A,T904A with compound (2S)-N-[(1S)-1-(4-{[6-(4-pyridinyl)-2-quinazolinyl]amino}phenyl)ethyl]-2-piperidinecarboxamide (Compound 2, IC_{50} 6.8 μM) resulted in crystals diffracting between 2.3 and 3.5 Å. Compound 1 a is kinase inhibitor that binds to multiple kinases, including FLT3, PDGFR, and FGFR. It was developed by Novartis and was subjected to clinical trials for the treatment of diverse types of cancer [18]. Crystals of the complexes were obtained in 0.1 M MES pH 6, 20% PEG 8 0000 with 0.2 M calcium acetate and 0.1 M BIS-TRIS pH 5.5–6.5, 20–25% PEG3350 with 0.2 M ammonium sulfate, respectively.

Crystal structure of human GCN2

The structures were solved by molecular replacement with yeast GCN2 as the search model (PDB code:1ZYD) [6] (N-lobe and C-lobes replaced separately). As shown in Figure 2, GCN2 largely adopts the canonical protein kinase fold consisting of a beta-stranded N-terminal lobe connected via the flexible hinge region (residues 801–806) to the alpha-helical C-terminal lobe. Similarly to PKR, the smaller N-lobe (residues 590–880) is preceded by a short noncanonical α-helix α0 (residues 584–589) and contains a five-stranded (β1–β5) twisted antiparallel β-sheet with a conserved helix αC (residues 628–642) linking β3–β4. The αC-helix is displaced from the canonical active arrangement and the large loop insert characteristic of the eIF2α kinase family members, truncated here to aid crystallization (residues 663–788), occurs between β4 and β5. The bulkier C-lobe (residues 807–1006) containing amino acids implicated in activation (Activation loop, A loop), and peptide substrate recognition (catalytic loop) is predominantly α-helical (αD-αI). The DFG motif in the N-terminal part of the activation loop adopts diverse conformations (as detailed subsequently) while the HRD motif (846–848) characteristic of the catalytic loop that anchors the substrate to be phosphorylated retains the classical active-like state independently of the arrangement of the A loop. A notable exception deviating from the canonical

Biochemical Journal (2020) 477 275–284
https://doi.org/10.1042/BCJ20190196

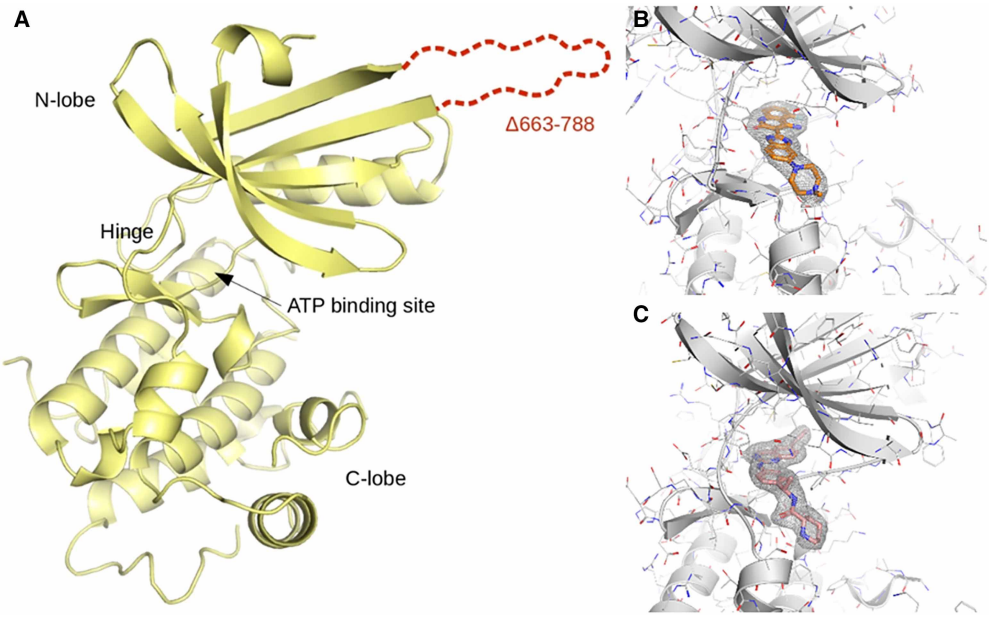

Figure 2. The crystal structure of human GCN2 kinase domain.

(**A**) Kinase domain canonical elements the N-terminal lobe, the C-terminal lobe and the hinge that connects the two kinase lobes are highlighted in the structure of GCN2. The insertion loop represented in red was removed to improve crystallizability. (**B**) Human GCN2 complexed to Compound 1. (**C**) Human GCN2 complexed to Compound 2.

configuration in the C-lobe is helix αG which is notably shifted, similarly to the structures of PKR and yeast GCN2 (Figure 2). Both inhibitors are clearly defined by difference electron density (Figure 2); they occupy the ATP binding site in the deep cleft between the N- and C-lobes of the kinase.

GCN2:Compound 1

4-amino-5-fluoro-3-[5-(4-methyl-1-piperazinyl)-1H-benzimidazol-2-yl]-2(1H)-quinolinone

GCN2 Complexed to dovitinib crystallized in space group $C222_1$ with 4 molecules in the asymmetric unit (cell parameters $A = 160$ Å, $B = 165$ Å, $C = 121$ Å). Compound 1 occupies the ATP binding site lined by an active-like conformation of the conserved N-terminal region of the activation loop of the kinase (Figure 2B). This conformation, so called, DFG-in, is characterized by the side chain of the aspartic acid pointing towards the ATP site where the phosphates of ATP would be and the phenylalanine pointing away from the site. The quinolinone group establishes hydrogen bonds with the hinge through the backbone carbonyl of Glu 803 and the amine of Cys 805 while a nitrogen from the benzimidazole interacts with the amide of Cys 805. In addition, there are hydrophobic contacts between the quinolone with Phe 855 and the gatekeeper residue Met 802. The methyl-piperazine tail extends out into the solvent channel; in two of the four molecules of the asymmetric unit, the piperazine is in position to establish a polar interaction with Asp 812. Protein:compound interactions can be seen in Supplementary Figure S4.

In two of the molecules, the activation loop is partially ordered (Asp 866 to Ala 874) and extend out into the solvent. There is the clear density for the DFG motif (Asp 866, Phe 867, and Gly 868) in all four molecules, and they are all poised in a DFG-in configuration. Interestingly, the critical catalytic salt bridge between Lys 619 in β-strand 3 and Glu 636 in the regulatory αC-helix, required by catalytic competent configurations of the KD, is absent. Instead, in all four molecules, Lys 619 is engaged in a salt bridge with the DFG-Asp 866 residue as in the dormant version of Src kinase [19]. Crystal structures of dovitinib complexes are available for FGFR1 [20], FGFR4 [21], and STK10 [22]. The superimposition of these structures reveals a similar binding mode, with most of the variation located in the solvent-exposed piperazine. Inhibitors that reach into the hydrophobic back pocket between the αC-helix and the β-sheet that forms the N-lobe of the kinase have been reported to stabilize kinase configurations where the catalytic bridge is broken and the C-helix is disengaged (αC-out).

Biochemical Journal (2020) **477** 275–284
https://doi.org/10.1042/BCJ20190196

Though dovitinib does not extend far into this pocket, the structures with FGFR4 and STK10 also lack the catalytic bridge. In these structures dovitinib behaves as a Type 1.5 inhibitor, that is, it binds to a DFG-in which notwithstanding represents an inactive conformation of the kinase.

GCN2:Compound 2

The GCN2:aminoquinazoline complex crystallized in space group P1 ($a = 73.80$, $b = 77.79$, $c = 101.69$; 89.86, 90.05, 68.58) with eight molecules in the ASU and it has been solved at 2.3 Å resolution. Six of these molecules (chains A,B,C,D,E,G) exhibit a DFG-out conformation, with a specific inactive arrangement of the DFG motif (Figure 2). Since the serendipitous discovery of type II inhibitor imatinib there has been great interest toward the development of inhibitors with comparable binding mode. Type II inhibitors additionally extend into an allosteric pocket directly adjacent to the ATP binding site by replacing the Phe of the conserved DFG motif, stabilizing the aforementioned 'DFG-out' configuration. This induced fit translates to slow binding kinetics and non-ATP competitive mode of inhibition. The susceptibility of kinases to type II inhibitors varies, and it remains unclear whether all kinases are able to undergo the required conformational rearrangement of the DFG motif. Our crystal structure shows GCN2 is able to adopt this conformation and therefore can accommodate type II inhibitors. The electron density for chain D allows for the substantial model building of activation loop: we can trace the segment from the Asp 866 until Ala875 and from Gln903 onwards.

In the other two molecules (chains F and H), the activation loop adopts an intermediate state between classical DFG-in and classical DFG-out (Figure 3). In typical DFG-in arrangements the aspartic acid points towards the ATP cleft, where the β phosphate would be located, while the phenylalanine points away from the cleft. In contrast, in typical DFG-out configurations the aspartic acid and phenylalanine point in almost opposite directions of DFG-in conformation. In chains F and H of human GCN2: Compound 2 complex, Asp 866 and Phe 867 point to the same overall direction: when compared with the DFG-in arrangement of the GCN2: Compound 1 structure, Asp 866 is rotated 40° and points towards the gatekeeper 802, while Phe867 is rotated upwards 100° and occupies a pocket above the side chain of C-helix Glu636 rather than stacking against the HRD His-846.

Structures capturing intermediates of the DFG flipping process have been reported elsewhere and named as DFG-up, pseudo DFG-out or atypical DFG-out [23]. They have reduced pocket volume in average when compared with classical DFG-out arrangements and are not compatible with a typical type II inhibitor [23]. In contrast with other non-classical DFG structures [24,25], the activation loop of this atypical DFG arrangement is positioned closer to the DFG-in conformation (RMSD 3.3 Å) (shown on the GCN2:dovitinib structure) than the classical DFG-out (RMSD 4.34 Å) GCN2:aminoquinazoline compound — chains A,B,C,D,E,G) (Figure 4).

The x-ray structure indicates that the aminoquinazoline group makes two hydrogen bonds to the hinge of the kinase through the backbone of the Cys 805. The pyridine extends to the start of the back cleft occupying the space in the vicinity of the gatekeeper Met 802 and can have a polar interaction with the backbone of the DFG-Phe (chain H) when the protein is in the DFG-up position. The piperazine ring is exposed to the solvent channel and can make a hydrogen bond with Asp 812. Interactions can be seen in Supplementary Figure S5.

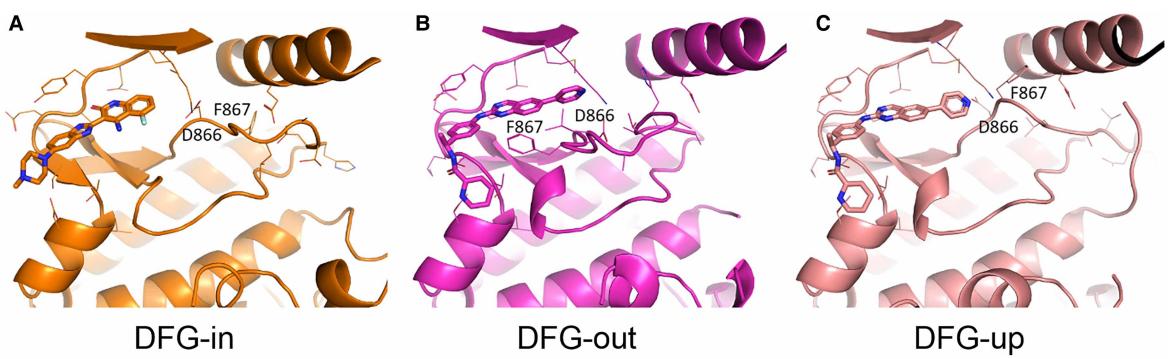

Figure 3. The different conformations adopted by the activation loop of human GCN2.

(**A**) Co-crystal structure of Compound 1 bound to GCN2 – the activation loop adopts the active DFG-in conformation. (**B**) and (**C**) Co-crystal structure of Compound 2 bound to GCN2 – in the different molecules within the asymmetric unit of this structure, the activation loop adopts either an inactive-DFG-out (**B**) or a DFG-up conformation (**C**).

Biochemical Journal (2020) **477** 275–284
https://doi.org/10.1042/BCJ20190196

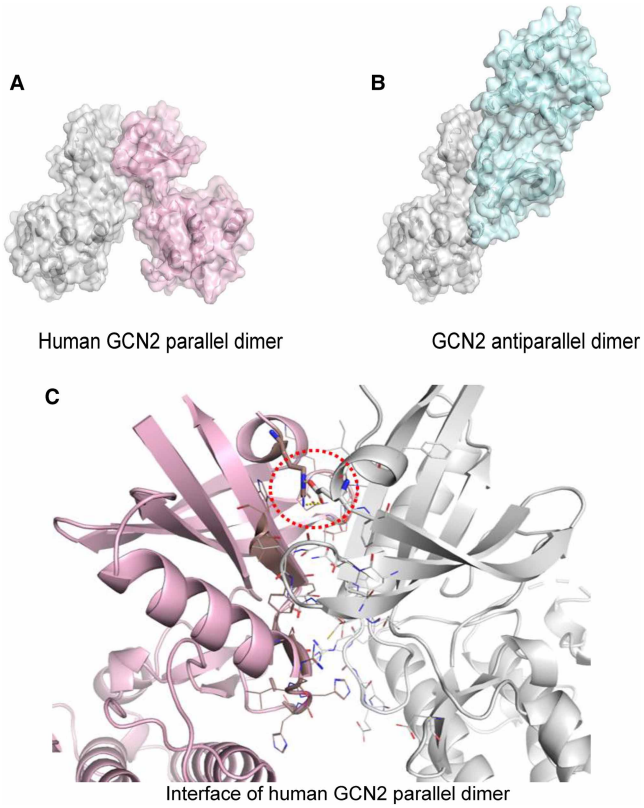

Figure 4. GCN2 dimeric organization.

The two top panels show a comparison of the dimeric structures of the kinase domains of (**A**) human GCN2 and (**B**) yeast GCN2. Human GCN2 dimerizes in a parallel orientation similar to PKR. Though yeast GCN2 dimerizes via a partially overlapping interface, the monomers are organized in antiparallel fashion. (**C**) Shows the interface of the back to back dimer highlighting the crucial electrostatic interaction between Arg 585 and Glu 589 (red dotted circle).

The quality of the density for the latter varies on different molecules in the asymmetric unit, and it is not clear the group is always in a good position to establish this interaction.

In short, this inhibitor binds to classical and non-classical DFG-out conformations of GCN2 while not extending far into the back cleft, and might be classified as a type II B inhibitor [26]. In general, these have a shorter residence time in relation to typical type II inhibitors (so-called type II A).

Regulation of human GCN2 activity

Structural studies based on yeast GCN2 postulate the kinase is inherently inactive because of the following characteristics: the catalytic salt bridge is broken and the C-helix is displaced out of its active position and there is an asparagine flap (Asn 793) that points toward the ATP binding site and sterically restricts access to it [6]. In addition, a network of interactions of residues in the vicinity of the hinge rigidifies the hinge interfering with the opening of the ATP cleft. In the human counterpart, one of the critical residues is an asparagine, which is replaced by a similarly bulky residue, Lys 807, that could perform a comparable function. The C-terminal portion of the hinge backbone that contains this residue in our structures is shifted 6 Å outwards when compared with the yeast GCN2 structure and in addition, the side chain of the lysine points away from the pocket, suggesting that this mechanism of autoinhibition might not be shared by humans. As we were not able to obtain a structure of human GCN2 in the absence of compounds, it could be possible that a similar mechanism does exist in humans and we do not observe the conformation simply because both inhibitors stabilize a version of the enzyme in which the flap is released. We, however, add that the MS analysis revealed autophosphorylation of the protein produced in *E. coli*, corroborating that the wild type KD of the human protein is not in an auto-inhibited state, at least when the insertion loop is not present.

In yeast GCN2, a single mutation from the arginine located in the C-terminal part of the hinge to Glycine (R794G — yeast numbering) increases the activity of the protein 75-fold [6]. This change was attributed to an enhancement of the flexibility of the hinge that interferes with the intramolecular interactions that keep the flap inside the ATP binding cleft and interfere with the interlobal movement required for substrate binding. Human GCN2 contains a serine (Ser 808) instead of an arginine at this position. This substitution might already be enough to decrease the rigidity of the hinge sufficiently to make the human GCN2 kinase more active than the yeast protein.

Dimerization has been reported to play a role in the activation of all four eIF2α kinases [27]: Previous crystal structures of the KDs of PERK and PKR revealed a back-to-back parallel dimer is formed by predominantly N-lobe interactions between residues conserved within the kinase family [28,10]. A crucial electrostatic interaction involves Arg 585 from one protomer with Glu 589 from the second protomer (human GCN2 numbering). Mutagenesis studies replacing either of the residues and thus interfering with the salt bridge formation decreased the activity of the GCN2, PERK, and PKR. Interestingly, the yeast GCN2 structure features symmetric back to back dimer which is distinct and instead organized in an antiparallel fashion (Figure 4). While most of the interface is common between the two dimeric configurations (which in both cases involve primarily the N-lobes of the kinases), the Arg–Glu pair are over 10 Å away from each other in the antiparallel dimer. Given that the yeast GCN2 KD is inherently inactive and thus adopts a non-productive arrangement, the current prevalent hypothesis is that the GCN2 dimerizes as an inactive antiparallel dimer similar to the PKR dimer and stays that way until the concentration of uncharged tRNA is increased and the HisRS histidyl-tRNA synthetase related domain binds to it, causing conformational change in the dimer that then re-organizes in the productive parallel fashion. Our structures show for the first time that a dimeric parallel conformation consistent with active PKR (Figure 4) can be indeed adopted by human GCN2 and strengthens the notion that GCN2 undergoes a transition from antiparallel to parallel dimer during its process of activation.

The dimeric PKR-like arrangement of GCN2 can be observed in both crystal forms: the dimers seen with compounds 1 and 2 look remarkably similar and can be superimposed with a low RMSD of 1.08 Å. When compared with the PKR parallel dimer, the GCN2 dimer is more closed (Supplementary Figure S6): the loops that connect the αC-helix and β4 are next to each other and engage into polar and apolar interactions, amounting to 13–17 intermolecular hydrogen bonds that include a network between Arg 650 of one protomer and the main chains of Tyr 651 and Leu 543 (in the GCN2:Compound 2 structure). The buried surface area of the interface amounts to 1958–2202 $Å^2$ in GCN2, depending on the crystal form, and is considerably larger than in PKR (1370–1760 $Å^2$).

In conclusion, the structures of human GCN2 presented in this study reveal a dimerization arrangement distinct from the yeast GCN2 dimeric assembly, corroborating the hypothesis that the GCN2 dimer transitions from antiparallel to parallel configuration upon activation. Activation of the GCN2 in response to amino acid deprivation is one mechanism by which cancer cells thrive in the nutrient stress setting of the tumor microenvironment [29]. Within this context, GCN2 remains interesting as an oncology target. Our structures highlight the plasticity of the activation loop and exhibit a rarer conformation that could be targeted in an effort to enhance the selectivity of GCN2 inhibitors.

Abbreviations

CTD, C-terminal dimerization domain; eIF2α, eukaryotic initiation factor 2; HisRS, histidyl-tRNA synthetase; KD, kinase domain; LCT ES-TOF, liquid chromatography electrospray ionization time-of-flight; PKD, pseudokinase domain.

Author Contribution

T.M.O. designed the constructs and carried out crystallization experiment and solved the structures. V.K. carried the biochemical experiments. S.C. performed sample characterization by SEC-MALS. J.J.W.H., M.L., and A.W.H. selected the compounds and progressed the chemistry. R.O. designed the constructs, developed protocols for purification, purified, and characterized the samples. The manuscript was written by T.M.O. with contributions from all authors.

Funding

This project was funded by AstraZeneca R&D.

Biochemical Journal (2020) **477** 275–284
https://doi.org/10.1042/BCJ20190196

Competing Interests

All authors are employees and shareholders of AstraZeneca, the funder of this study.

References

1 Shenolikar, S. (2012) *Protein Phosphorylation in Health and Disease*, Academic Press, Orlando, FL.
2 Timosenko, E., Hadjinicolaou, A.V. and Cerundolo, V. (2017) Modulation of cancer-specific immune responses by amino acid degrading enzymes. *Immunotherapy* **9**, 83–97 https://doi.org/10.2217/imt-2016-0118
3 Castilho, B.A., Shanmugam, R., Silva, R.C., Ramesh, R., Himme, B.M. and Sattlegger, E. (2014) Keeping the eIF2 alpha kinase Gcn2 in check. *Biochim. Biophys. Acta* **1843**, 1948–1968 https://doi.org/10.1016/j.bbamcr.2014.04.006
4 Inglis, A.J., Masson, G.R., Shao, S., Perisic, O., McLaughlin, S.H., Hegde, R.S. et al. (2019) Activation of GCN2 by the ribosomal P-stalk. *Proc. Natl. Acad. Sci. U.S.A.* **116**, 4946–4954 https://doi.org/10.1073/pnas.1813352116
5 He, H., Singh, I., Wek, S.A., Dey, S., Baird, T.D., Wek, R.C. et al. (2014) Crystal structures of GCN2 protein kinase C-terminal domains suggest regulatory differences in yeast and mammals. *J. Biol. Chem.* **289**, 15023–15034 https://doi.org/10.1074/jbc.M114.560789
6 Padyana, A.K., Qiu, H., Roll-Mecak, A., Hinnebusch, A.G. and Burley, S.K. (2005) Structural basis for autoinhibition and mutational activation of eukaryotic initiation factor 2α protein kinase GCN2. *J. Biol. Chem.* **280**, 29289–29299 https://doi.org/10.1074/jbc.M504096200
7 Nameki, N., Yoneyama, M., Koshiba, S., Tochio, N., Inoue, M., Seki, E. et al. (2004) Solution structure of the RWD domain of the mouse GCN2 protein. *Protein Sci.* **13**, 2089–2100 https://doi.org/10.1110/ps.04751804
8 Qiu, H., Dong, J., Hu, C., Francklyn, C.S. and Hinnebusch, A.G. (2001) The tRNA-binding moiety in GCN2 contains a dimerization domain that interacts with the kinase domain and is required for tRNA binding and kinase activation. *EMBO J.* **20**, 1425–1438 https://doi.org/10.1093/emboj/20.6.1425
9 Lageix, S., Rothenburg, S., Dever, T.E. and Hinnebusch, A.G. (2014) Enhanced interaction between pseudokinase and kinase domains in Gcn2 stimulates eIF2α phosphorylation in starved cells. *PLoS Genet.* **10**, e1004326 https://doi.org/10.1371/journal.pgen.1004326
10 Dar, A.C., Dever, T.E. and Sicheri, F. (2005) Higher-order substrate recognition of eIF2α by the RNA-dependent protein kinase PKR. *Cell* **122**, 887–900 https://doi.org/10.1016/j.cell.2005.06.044
11 Axten, J.M., Medina, J.R., Feng, Y., Shu, A., Romeril, S.P., Grant, S.W. et al. (2012) Discovery of 7-methyl-5-(1-{[3-(trifluoromethyl)phenyl] acetyl}-2,3-dihydro-1*H*-indol-5-yl)-7*H*-pyrrolo[2,3-*d*]pyrimidin-4-amine (GSK2606414), a potent and selective first-in-class inhibitor of protein kinase R (PKR)-like endoplasmic reticulum kinase (PERK). *J. Med. Chem.* **55**, 7193–7207 https://doi.org/10.1021/jm300713s
12 Hinnebusch, A.G. (2005) eIF2α kinases provide a new solution to the puzzle of substrate specificity. *Nat. Struct. Mol. Biol.* **12**, 835–838 https://doi.org/10.1038/nsmb1005-835
13 Cole, J.L. (2007) Activation of PKR: an open and shut case? *Trends Biochem. Sci.* **32**, 57–62 https://doi.org/10.1016/j.tibs.2006.12.003
14 Deng, J., Harding, H.P., Raught, B., Gingras, A.-C., Berlanga, J.J., Scheuner, D. et al. (2002) Activation of GCN2 in UV-irradiated cells inhibits translation. *Curr. Biol.* **12**, 1279–1286 https://doi.org/10.1016/S0960-9822(02)01037-0
15 Shapiro, A.B., Walkup, G.K. and Keating, T.A. (2009) Correction for interference by test samples in high-throughput assays. *J. Biomol. Screen.* **14**, 1008–1016 https://doi.org/10.1177/1087057109341768
16 Emsley, P. and Cowtan, K. (2004) *Coot*: model-building tools for molecular graphics. *Acta Crystallogr. D Biol. Crystallogr.* **60**, 2126–2132 https://doi.org/10.1107/S0907444904019158
17 Bricogne, G., Blanc, E., Brandl, M., Flensburg, C., Keller, P., Paciorek, W. et al. (2017) *Buster Version 2.11.2*, Global Phasing Ltd, Cambridge, U.K.
18 Musolino, A., Campone, M., Neven, P., Denduluri, N., Barrios, C.H., Cortes, J. et al. (2017) Phase II, randomized, placebo-controlled study of dovitinib in combination with fulvestrant in postmenopausal patients with HR+, HER2− breast cancer that had progressed during or after prior endocrine therapy. *Breast Cancer Res.* **19**, 18 https://doi.org/10.1186/s13058-017-0807-8
19 Roskoski, R. (2015) Src protein-tyrosine kinase structure, mechanism, and small molecule inhibitors. *Pharmacol. Res.* **94**, 9–25 https://doi.org/10.1016/j.phrs.2015.01.003
20 Klein, T., Vajpai, N., Phillips, J.J., Davies, G., Holdgate, G.A., Phillips, C. et al. (2015) Structural and dynamic insights into the energetics of activation loop rearrangement in FGFR1 kinase. *Nat. Commun.* **6**, 7877 https://doi.org/10.1038/ncomms8877
21 Lesca, E., Lammens, A., Huber, R. and Augustin, M. (2014) Structural analysis of the human fibroblast growth factor receptor 4 kinase. *J. Mol. Biol.* **426**, 3744–3756 https://doi.org/10.1016/j.jmb.2014.09.004
22 Elkins, J. M. 2017. Human STK10 bound to dovitinib. PDB databank (to be published) https://doi.org/10.2210/pdb5owq/pdb
23 Vijayan, R.S.K., He, P., Modi, V., Duong-Ly, K.C., Ma, H., Peterson, J.R. et al. (2015) Conformational analysis of the DFG-out kinase motif and biochemical profiling of structurally validated type II inhibitors. *J. Med. Chem.* **58**, 466–479 https://doi.org/10.1021/jm501603h
24 Dodson, C.A., Kosmopoulou, M., Richards, M., Atrash, B., Bavetsias, V., Blagg, J. et al. (2010) Crystal structure of an Aurora-A mutant that mimics Aurora-B bound to MLN8054: insights into selectivity and drug design. *Biochem. J.* **427**, 19–28 https://doi.org/10.1042/BJ20091530
25 Kuglstatter, A., Wong, A., Tsing, S., Lee, S.W., Lou, Y., Villaseñor, A.G. et al. (2011) Insights into the conformational flexibility of Bruton's tyrosine kinase from multiple ligand complex structures. *Protein Sci.* **20**, 428–436 https://doi.org/10.1002/pro.575
26 Roskoski, R. (2016) Classification of small molecule protein kinase inhibitors based upon the structures of their drug-enzyme complexes. *Pharmacol. Res.* **103**, 26–48 https://doi.org/10.1016/j.phrs.2015.10.021
27 Hernández, G. and Jagus, R. (2016) *Evolution of the Protein Synthesis Machinery and Its Regulation*, Springer, Cham, Switzerland
28 Cui, W., Li, J., Ron, D. and Sha, B. (2011) The structure of the PERK kinase domain suggests the mechanism for its activation. *Acta Crystallogr. D Biol. Crystallogr.* **67**, 423–428 https://doi.org/10.1107/S0907444911006445
29 Lehman, S.L., Ryeom, S. and Koumenis, C. (2015) Signaling through alternative Integrated Stress Response pathways compensates for GCN2 loss in a mouse model of soft tissue sarcoma. *Sci. Rep.* **5**, 11 781https://doi.org/10.1038/srep11781